Photoelectrochemical Water Oxidation Characteristics of Anodically Fabricated TiO 2 Nanotube Arrays: Structural and Optical Properties

ARTICLE *in* THE JOURNAL OF PHYSICAL CHEMISTRY C · JULY 2010

Impact Factor: 4.77 · DOI: 10.1021/jp1037014

2 AUTHORS:

Nageh K. Allam
Massachusetts Institute of Technology
95 PUBLICATIONS **1,757** CITATIONS
SEE PROFILE

Mostafa A El-Sayed
Georgia Institute of Technology
676 PUBLICATIONS **54,961** CITATIONS
SEE PROFILE

Photoelectrochemical Water Oxidation Characteristics of Anodically Fabricated TiO_2 Nanotube Arrays: Structural and Optical Properties

Nageh K. Allam[†] and Mostafa A. El-Sayed*

Laser Dynamics Laboratory, School of Chemistry and Biochemistry, Georgia Institute of Technology, Atlanta, Georgia 30332-0400

Received: April 24, 2010; Revised Manuscript Received: June 4, 2010

There are currently immense needs to optimize low-cost materials, such as TiO_2, so they can efficiently split water photoelectrochemically into hydrogen and oxygen, thus providing a clean energy fuel. To this end, the nature of the crystalline phase and the dimension of the photocatalyst are of crucial significance. In this study, films of 7 μm long titania nanotube arrays were fabricated via anodization of titanium foil in formamide electrolytes containing NH_4F and H_3PO_4. Upon annealing the as-anodized nanotubes, the anatase-to-rutile phase transformation was found to start at 550 °C, which is about 120 °C above the temperature observed for the 500 nm long nanotube films, with the nanotube films remaining stable up to 580 °C. Analysis of the variation of crystallite size with annealing temperature along with XPS analysis of the films was used to investigate the reason behind this observation. UV−vis measurements showed that the absorption edges of the annealed samples were red shifted from that of the as-anodized sample. The stabilization of the anatase phase up to 550 °C, while keeping the tubular structure in place, is very significant as anatase is the most photoactive polymorph of titania. Besides, the 7 μm long nanotubular structure provides a large surface medium for light utilization through scattering. Used as photoanodes to photoelectrochemically split water, the 580 °C crystallized nanotube arrays showed a three-electrode photoconversion efficiency of 10% under UV illumination (100 mW/cm^2, 320−400 nm, 1 M KOH).

1. Introduction

Fujishima and Honda discovered the photosplitting of water on TiO_2 thin films in 1972, which opened a new vista for hydrogen and oxygen production from water using sunlight.[1] Recently, due to the environmental and energy concerns related to fossil fuel dependence, this approach for solar energy conversion has once again been revisited with many research efforts aimed toward the optimization of the material architecture to enhance its efficiency for hydrogen production through photoelectrochemical water splitting.[2–4] As numerous major advances in research and technology over the past decade or two have been made possible by the successful development of nanostructures,[5] various avenues have been used to fabricate a diversity of titania nanoarchitectures.[6] Although many of those fabrication routes are complicated due to the use of templates or the nature of the involved chemical processes, it has recently been demonstrated that self-organized vertically oriented titanium dioxide nanotube arrays can be fabricated using a simple anodization technique.[7] This technique can yield nanotubes of controlled diameters, wall thicknesses and lengths.[3,8–18] However, all anodically fabricated TiO_2 nanotube arrays to date are amorphous, with a minor number of trial studies toward the direct fabrication of crystalline titania nanotubes with limited success.[19,20] This property limits the application of these nanotubes as both conductivity and mechanical strength are very low. Therefore, before utilization of these amorphous nanotubes in different applications, factors, such as the crystalline nature of the structure and stability of the desired crystalline phase as well as the stability of the structure itself, must be examined. For example, the anatase phase of titania is preferred in dye-sensitized solar cells and catalysis because it is photoactive, whereas rutile is mostly used in the area of dielectrics and high-temperature oxygen gas sensors.[6,21] On the basis of the fact that titanium exhibits a capacity for dissolving a considerable amount of oxygen,[22] most of the crystallization methods used for the anodically fabricated TiO_2 nanotubes involve annealing the material at high temperature in an oxygen atmosphere.[23] Varghese and co-workers had studied the crystallization and thermal stability of titania nanotubes up to 500 nm in length.[23] However, it is now well realized that the nanotube length is of crucial significance in many applications.[11] Therefore, it is necessary to study the crystalinity and thermal stability of relatively long nanotube arrays (several micrometers in length) to determine the optimal annealing conditions for TiO_2 nanotube arrays in order to perform as an efficient material. Herein, we report on the crystallinity and thermal stability of 7 μm long nanotube arrays as well as the effect of this treatment on their optical and photoelectrochemical water oxidation properties.

2. Experimental Section

Prior to anodization, pure titanium foil samples (2.0 × 1.0 cm × 0.25 mm) were ultrasonically cleaned with acetone, followed by a deionized (D.I.) water rinse. The anodization was performed in a two-electrode electrochemical cell with the titanium foil as the working electrode and platinum foil as the counter electrode at room temperature (approximately 22 °C) at 20 V for 20 h in a formamide-based electrolyte containing 0.2 M NH_4F, 1 M H_3PO_4, and 3 vol % H_2O. An Agilent E3612A-CFG001 dc power supply was used for potentiostatic anodization. After anodization, the samples were rinsed thor-

* To whom correspondence should be addressed. E-mail: mostafa.el-sayed@chemistry.gatech.edu.
[†] Permanent address: Electrochemistry Lab., National Research Center, Dokki, Cairo 12622, Egypt. E-mail: Nageh.allam@gmail.com.

10.1021/jp1037014
Published on Web 06/21/2010

oughly with deionized water and isopropyl alcohol and then dried under a stream of nitrogen. The as-anodized samples were crystallized by oxygen annealing at different temperatures with heating and cooling rates of 1 °C/min. The morphology of the anodized samples was examined using a field emission scanning electron microscope (FESEM). X-ray photoelectron spectroscopy (XPS) experiments were performed on the TiO_2 films using a Thermo Scientific K-Alpha XPS with an Al anode. Photoelectrons were collected in hybrid mode over an analysis area of about 1.5 mm^2, with the plane of the sample surface normal to the analyzer entrance. Spectra were charge referenced to O 1s at 532 eV. The crystalline phases were detected and identified by a glancing angle X-ray diffractometer (GAXRD) on an X'Pert PRO MRD with a copper source.

The optical characterization of the films was performed using a Shimadzu UV-3101PC UV−vis-NIR spectrophotometer. Photoelectrochemical properties were investigated in 1.0 M KOH solution using a three-electrode configuration with a TiO_2 nanotube array photoanode, saturated Ag/AgCl as a reference electrode, and platinum foil as a counter electrode. A scanning potentiostat (CH Instruments, model CH 660D) was used to measure dark and illuminated currents at a scan rate of 10 mV/s. A 50 W mercury arc lamp (Exfo lite) was used as the light source, with optical filters used to restrict the incident light to UV wavelengths between 320 and 400 nm.

3. Results and Discussion

3.1. Morphological and Structural Properties. Figure 1 shows FESEM images of the as-fabricated nanotube arrays. It can be seen that the nanotube array is uniform over the entire substrate. The cross-sectional view of the nanotube arrays is shown in Figure 1b. The tubular structure with a nearly uniform wall thickness throughout the length of the tube is evident from the figure. The as-prepared samples were found to have a length of approximately 7 ± 0.2 μm, an outer diameter of 85 ± 1 nm, and a wall thickness of 16.5 ± 1 nm.

Figure 2 shows the XRD patterns of the as-anodized as well as the annealed samples at different temperatures in dry oxygen ambient. As the two low-energy surfaces of anatase and rutile are (101) and (110), respectively,[21] only diffractions from these surfaces are shown in Figure 2. The as-anodized nanotube arrays were found to be amorphous. In the diffraction patterns, the anatase phase starts to appear at 300 °C as the 230 °C annealed sample was amorphous with only a small reflection appearing at $2\theta \sim 40°$ that can be related to the titanium substrate (not shown). Titania is an oxide with structural complexity due to the bond flexibility giving rise to polymorphs with the same chemistry and/or similar free energy of formation and mixed valence compounds with infinitely adaptive physical structures that accommodate changes in stoichiometry.[24] Therefore, it is not surprising that nanotube films grown and/or annealed at low temperature are amorphous. The intensity of the anatase (101) increases with increasing temperature up to 550 °C. Near 550 °C, the rutile phase emerges in the X-ray diffraction pattern. After this temperature, the relative intensity of the rutile (110) peak, with respect to the anatase (101) peak, increased. Note that the anatase-to-rutile transformation starts near 430 °C for the 500 nm long nanotubes studied by Varghese and coworkers[23] (i.e., at 120 °C lower than that observed in our study), confirming that the nanotube length is a critical factor in the phase transformation process and consequently on the properties of the material.

Although the rutile ratio increases with increasing the annealing temperature beyond 550 °C, complete transformation

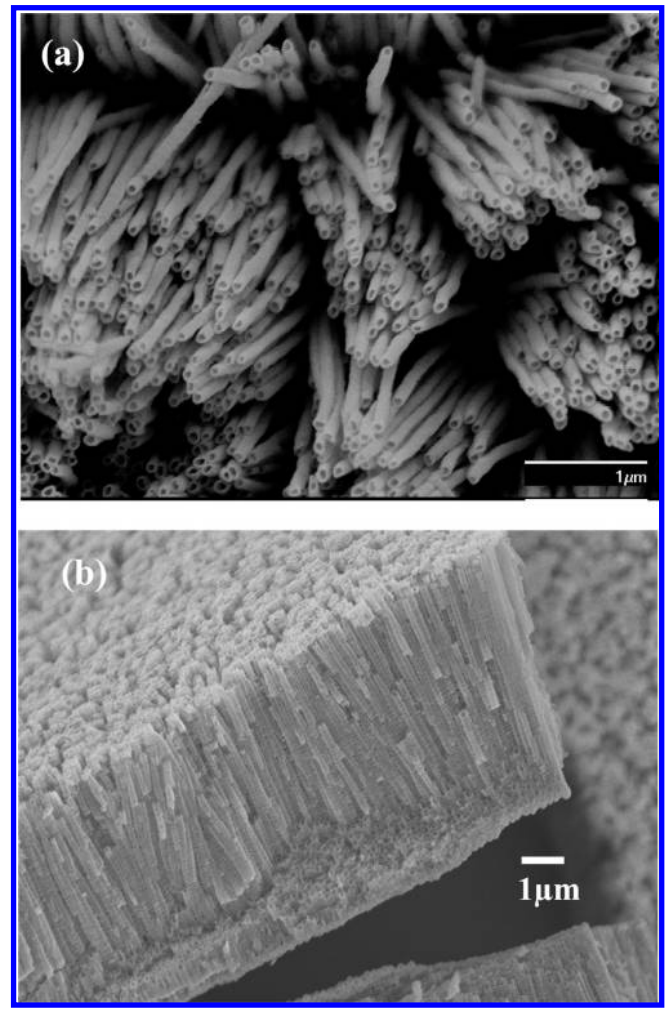

Figure 1. (a) FESEM top-view image of the as-fabricated TiO_2 nanotube arrays upon anodizing Ti foil in a formamide-based electrolyte containing 0.2 M NH_4F, 1 M H_3PO_4, and 3 vol % H_2O at 20 V for 20 h. (b) The corresponding cross-sectional view.

to rutile does not occur even upon annealing to 700 °C. This is in contrast to short titania nanotubes[23] as well as thin films where complete transformation occurs at 620 and 580 °C, respectively, as shown in Figure 5 for titania thin films. Zhang and Banfield reported that small crystallite sizes (<14 nm) will energetically favor remaining in the anatase phase rather than transforming to the rutile phase.[25] They related this phase transformation retardation to the lower surface free energy for the anatase phase as compared with that of the rutile phase. To test the validity of this argument to our material, the variation of the size of the anatase and rutile crystallites (D) with temperature was calculated using the Scherrer equation[26]

$$D = \frac{0.9\lambda}{\mathrm{FWHM}\cos(\theta)} \quad (1)$$

where λ is the wavelength of Cu Kα radiation (1.5418 Å), 0.9 is the Scherrer constant, θ is the Bragg reflection angle, and FWHM is the full width at half-maximum intensity of the anatase (101) peak or rutile (110) peak. The relative standard deviation of the determined average particle size is ~7%. The instrument broadening was corrected for using NIST 640c silicon. Figure 3 shows that the grain size of the rutile phase progressively increased with temperature after its nucleation. In contrast, the average size of the anatase grains shows a

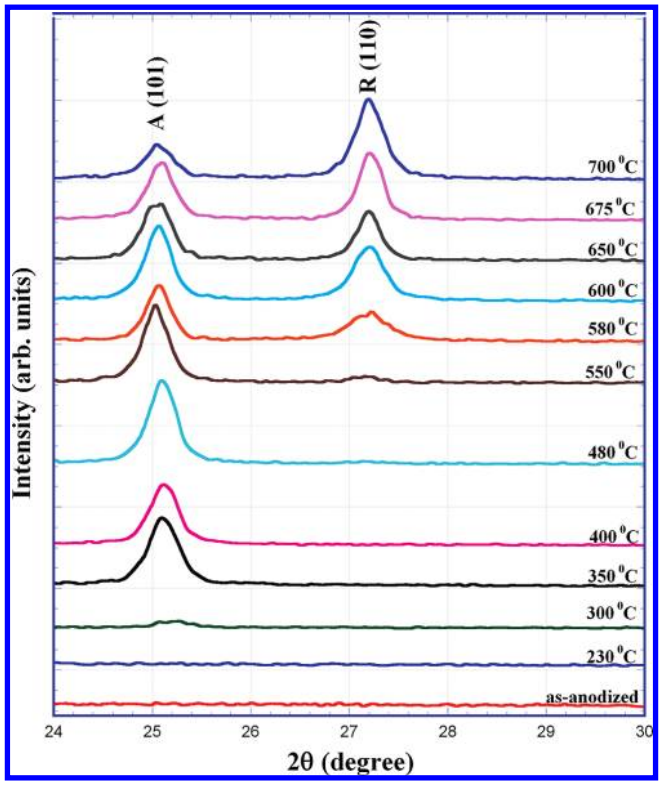

Figure 2. Glancing angle X-ray diffraction patterns of 7 μm long nanotube arrays as a function of annealing temperature in dry oxygen ambient.

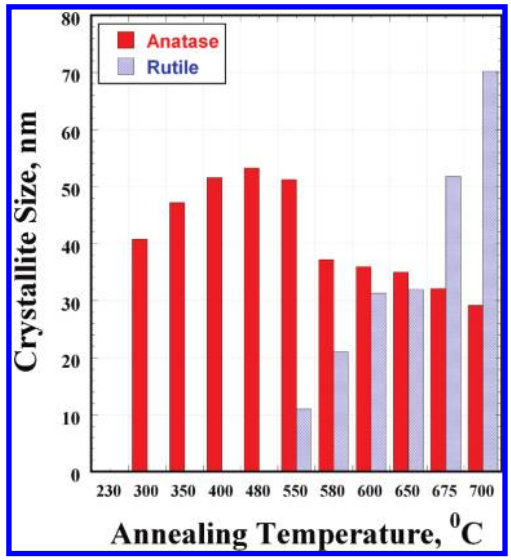

Figure 3. Variation of the anatase (101) and rutile (110) crystallite sizes of the annealed TiO_2 nanotube samples with the annealing temperature.

decreasing trend starting at the temperature where the rutile phase starts to appear. This might indicate that, above 550 °C, the large anatase grains transform into rutile with the smaller grains remaining anatase.

Evolution of the nanotube architecture as a result of high-temperature annealing shows that the nanotubular structure is retained up to around 580 °C; see Figure 4a. No discernible changes in the pore diameter or wall thickness were observed even after annealing for 6 h at this temperature. However, annealing at higher temperatures (>600 °C) was accompanied with structural collapse of some portions of the nanotubes (Figure 4b), as evidenced by shortening of the nanotube length.

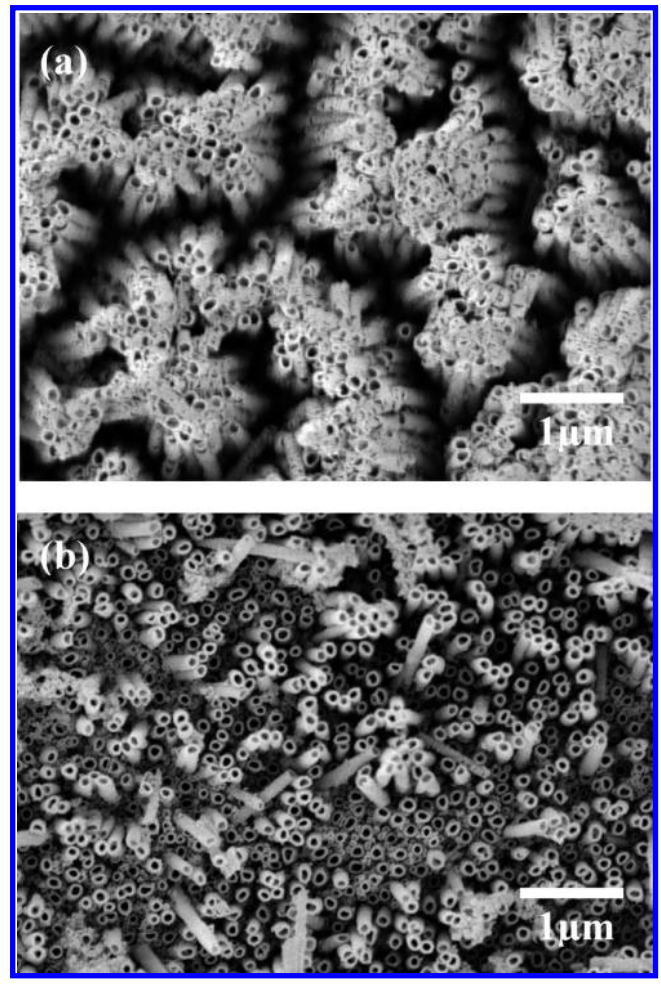

Figure 4. Effect of annealing temperature on the surface morphology of TiO_2 nanotube array samples annealed in O_2 ambient at (a) 580 and (b) 620 °C.

It is noteworthy to mention that the tubular structure does not disappear (collapse) completely even upon annealing at 700 °C. This can be used to explain the existence of anatase (101) peaks in the XRD patterns for samples annealed at all temperatures as it is believed that the anatase crystallites form within the tube walls.[23]

These results showed that the fabricated titania nanotube architectures remain stable up to temperatures near 580 °C when annealed in oxygen, without any notable change in the pore diameter, wall thickness, or tube length. The protrusions emanating from the underlying titanium support in the form of rutile crystallites is believed to be the major cause of the material degradation above this temperature. Were the appeared rutile peaks in the XRD pattern of the annealed samples associated with the supporting titanium substrate? To investigate this possibility, bare titanium foil samples were annealed under the same conditions to those used to anneal the nanotubes. XRD of the substrate showed an almost similar result as that observed in the case of a nanotube sample subjected to identical treatment, but the relative intensity of the rutile (110) peak to the anatase (101) peak was found to be higher in the case of bare titanium foil even at lower temperatures compared with those of the nanotube samples; see Figure 5. Note that complete transformation to rutile is observed at a temperature near 580 °C, which was not the case for the annealed nanotube arrays. Hence, it is clear that part or all of the rutile phase observed in the XRD patterns of the nanotube array annealed samples (Figure 2) is

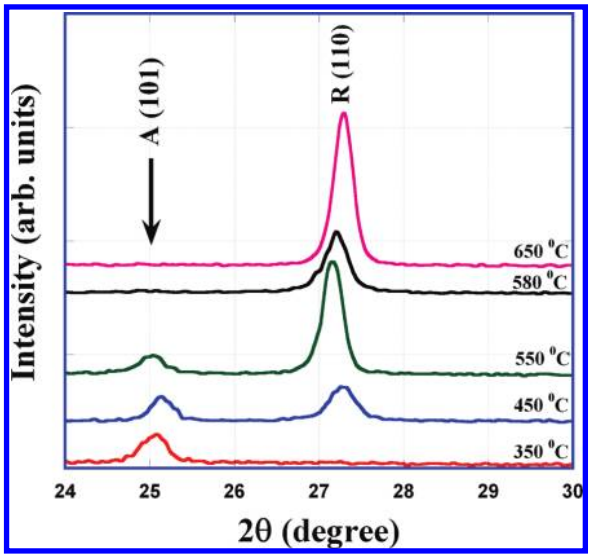

Figure 5. Glancing angle X-ray diffraction patterns of bare titanium foil as a function of annealing temperature in oxygen ambient.

from the substrate. Another observation that supports this possibility is the lower anatase crystallite size above 480 °C (Figure 3) as compared with that at temperatures ≤ 480 °C. This smaller crystallite size indicates the possibility that the larger anatase crystallites in the nanotube−titania support interface region were converted into rutile, leaving those on the nanotube walls unaffected.

3.1.1. Reason for the Observed Slow Phase Transformation. It seems that our results are not in agreement with that of Zhang and Banfield[25] as the minimum anatase crystallite size we observed was greater than 14 nm. To get more information about the crystal structure of the nanotubes and to explore the reason behind the slow phase transformation, we have performed XPS analyses of the nanotubes annealed at different temperatures. The formation of oxide is evident from the O 1s and Ti 2p peaks with the molar ratio of Ti/O being close to the stoichiometric proportion. Note that both Ti $2p_{3/2}$ and $2p_{1/2}$ peaks are observed (Figure 6a) with a separation of 5.7 eV, which confirm the presence of Ti^{4+}.[27] One important observation was the appearance of a peak at 134.8 eV that can be assigned to P 2p that might be incorporated into the tubes from the anodization electrolyte containing 1 M H_3PO_4; see Figure 6b. This can be used to explain the observed slow anatase-to-rutile phase transformation in our system as the incorporation of higher valence cations into TiO_2 is expected to result in the formation of interstitial Ti^{3+} cations that suppresses atomic transport in the anatase phase. Xu and co-workers[28] have very recently shown that the incorporation of P into their sol−gel fabricated TiO_2 structures greatly suppresses anatase-to-rutile phase transformation as phosphates are known to adsorb strongly on titanium oxide surfaces. To validate this assumption, we have followed the change in the XPS peak intensity for samples annealed at different temperatures. In general, the intensity of the P 2p peak was found to decrease with increasing the annealing temperature. However, this decrease was minimal up to about 550 °C and then very rapid beyond this temperature. This is in a very good agreement with our X-ray results confirming the role of incorporated/doped P in stabilizing the anatase phase. On the other hand, a very well-defined reflection was observed at 685.4 eV which is quite shifted from the reflection usually seen, between 683 and 684 eV, for free fluoride ions.[27] This peak can be related to the presence of a TiF_6^{2-} complex,[27] which is well-known to form during anodization of Ti in fluoride-containing media. This shift is expected as the binding energy of electrons in TiF_6^{2-} is expected to be higher than that in TiO_2 as fluoride is more electronegative than oxygen. As this observation was interesting, we aimed to follow the change in the composition of this complex as a function of annealing temperature. Figure 6c shows the change in the XPS peak intensity of the TiF_6^{2-} complex as a function of annealing temperature. It is interesting to note that the intensity of this peak decreases with increasing the annealing temperature; that is, fluoride ions are gradually released from the nanotubes. However, it is not completely removed even upon annealing at 600 °C. This remaining fluoride layer on crystallized nanotube array films is expected to be very important for some applications, such as quantum dot solar cells. For example, Diguna and co-workers showed that the system TiO_2/F/CdSe is superior to the system TiO_2/CdSe when used for solar cell assembly.[29]

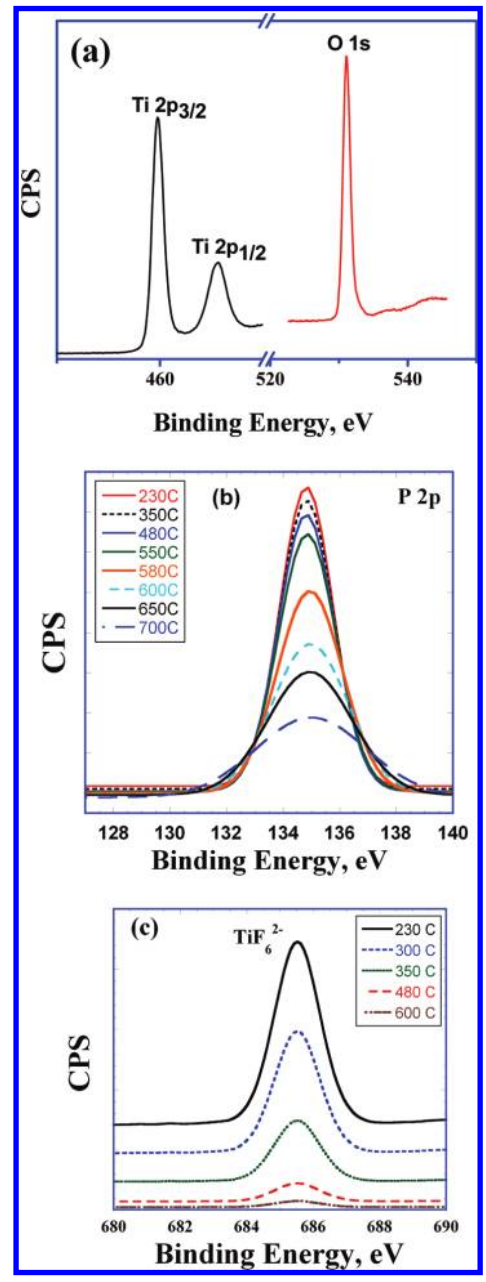

Figure 6. XPS spectra for annealed TiO_2 nanotube films showing (a) Ti 2p and O 1s and (b) P 2p and (c) F 1s.

3.2. Optical Properties. Figure 7a shows the diffuse reflectance spectra (DRS UV−vis) of the as-anodized as well

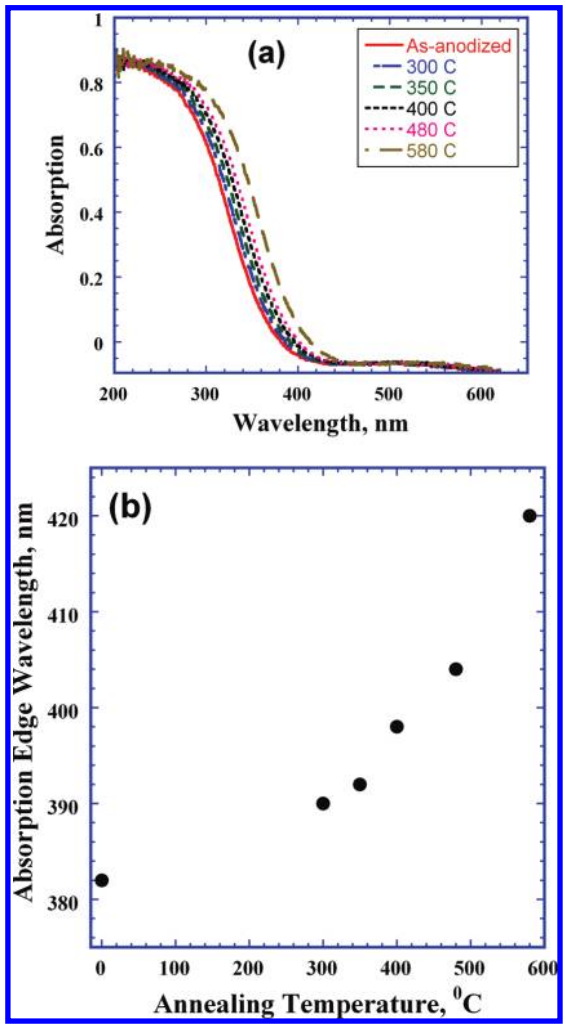

Figure 7. (a) Variation of the DRS UV−vis spectra of TiO_2 nanotube samples with the annealing temperature and (b) the corresponding variation of the absorption edge with temperature. Note that the zero temperature in (b) refers to the as-anodized sample.

as annealed TiO_2 nanotube array films. In general, the absorption edge shows a red shift with increasing the annealing temperature, which can be related to the enhancement of crystallization with increasing the annealing temperature. Figure 7b shows the variation of the absorption edge wavelength as a function of annealing temperature. The shift is minimal for all samples annealed below 580 °C and seriously increased for the sample annealed at 580 °C. However, on the basis of the band gap of TiO_2, the absorption band edge should not be more than 413.3 nm (corresponding to 3 eV for rutile phase). The little bit of red shift more than 413 nm seen for the sample annealed at 580 °C can be related to the synergistic effect between the low-band-gap rutile phase and the presence of P ions. This is in parallel with Xu and coworkers,[28] who showed that P-doping resulted in a red shift in the absorption edge of titania powders depending on the amount of P ions.

3.3. Photoelectrochemical Water Oxidation. Figure 8a shows the variation of the steady-state photocurrent density with the annealing temperature of 7 μm nanotube arrays annealed at different temperatures under UV (320−400 nm) illumination with an intensity of 100 mW/cm^2 on the surface; the dark current in all cases is approximately 10^{-7} to 10^{-6} A. The photocurrent increases with increasing annealing temperature to 580 °C, after which it decreases, with samples

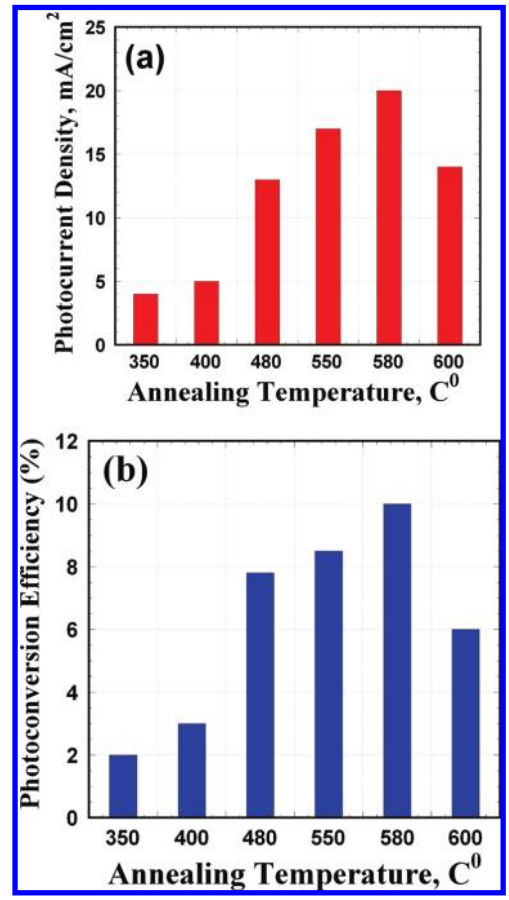

Figure 8. (a) The steady-state photocurrent generated from 7 μm long nanotube arrays under an applied voltage of 0.5 V in 1 M KOH with respect to annealing temperature and (b) the corresponding photoconversion efficiencies.

annealed at 625 °C showing a lower photocurrent than samples annealed at 550 °C.

The corresponding light energy-to-chemical energy conversion (photoconversion) efficiencies (η) (Figure 8b) were calculated using eq 2[2]

$$\eta\% = [(\text{total power output} - \text{electrical power input})/\text{light power input}] \times 100$$

$$\eta(\%) = \frac{j_P(1.23 - |E_{measured} - E_{ocp}|)}{I_0} \times 100 \qquad (2)$$

where j_p is the photocurrent density, I_0 is the intensity of incident light, $E_{measured}$ is the measured voltage, and E_{ocp} is the open-circuit potential.

An efficiency of about 10% was obtained for samples annealed at 580 °C. The increase in photocurrent and efficiency can be related to the increased crystallinity of the nanotube walls, with the reduction of the amorphous regions and grain boundaries, in turn, reducing the number of charge carrier recombination centers.[21,30,31] However, at temperatures near 625 °C, the densification of the bottom part of the nanotubes, as indicated by the increase in the rutile-to-anatase ratio (Figure 2), starts isolating the undestroyed nanotubes from the metal substrate, reducing the number of charge carriers reaching the electrode.[20] Also, the low conversion efficiency at high annealing temperatures can be related, in part, to the partial structural collapse of the tubes; see Figure 4b.

4. Summary and Conclusions

Room-temperature anodization of titanium foil at 20 V for 20 h in formamide electrolytes containing 0.2 M NH_4F, 1 M H_3PO_4, and 3 vol % H_2O resulted in the formation of 7 μm long amorphous TiO_2 nanotube array films. Annealing the as-anodized nanotubes resulted in their crystallization with the anatase-to-rutile phase transformation initiating at 550 °C. This transformation temperature is about 120 °C above that observed for the 500 nm long nanotube films. Analysis of the variation of crystallite size with annealing temperature revealed the increase in anatase crystallite sizes with increasing temperature up to 480 °C, after which it decreases with the emergence of rutile crystallites. However, the anatase crystallite sizes were greater than 14 nm in all cases, indicating that the model proposed by Zhang and Banfield[25] is not applicable to our system, although it was applicable to the 500 nm long nanotube films.[23] XPS analysis showed the incorporation of P ions into the TiO_2 films, which was used to explain the retardation of the anatase-to-rutile phase transformation. TiO_2 nanotube arrays were found to be stable up to ~580 °C, with higher temperatures resulting in the oxidation of the titanium support, which disturbed the nanotube architecture, causing it to partially and gradually collapse and densify. DRS UV−vis measurements showed that the absorption edges of the annealed samples were red shifted from that of the as-anodized sample. The 580 °C thermally annealed TiO_2 electrode showed a maximum photoconversion efficiency of 10% under UV illumination (100 mW/cm^2, 320−400 nm, 1 M KOH) when used as a photoanode to split water photoelectrochemically.

Acknowledgment. We thank Prof. Jiri Janata and Dr. Mira Josowicz from Georgia Tech, School of Chemistry and Biochemistry, for using their photoelectrochemical system. N.K.A. would like to thank the RAK-CAM Foundation for a Sheikh Saqr Al Qasimi postdoctoral fellowship, and M.A.E. would like to thank the DOE for Grant No. DE-FG02-97ER14799.

References and Notes

(1) Fujishima, A.; Honda, K. *Nature* **1972**, *238*, 37.
(2) Grimes, C. A.; Varghese, O. K.; Ranjan, S. *Light, Water, Hydrogen: The Solar Production of Hydrogen by Water Photoelectrolysis*; Springer: Norwell, MA, 2007.
(3) Shankar, K.; Basham, J. I.; Allam, N. K.; Varghese, O. K.; Mor, G. K.; Feng, X. J.; Paulose, M.; Seabold, J. A.; Choi, K. S.; Grimes, C. A. *J. Phys. Chem. C* **2009**, *113*, 6327.
(4) Allam, N. K.; Shankar, K.; Grimes, C. A. *J. Mater. Chem.* **2008**, *18*, 2341.
(5) Rao, C. N. R., Müller, A., Cheetham, A. K., Eds. *Nanomaterials Chemistry: Recent Developments and New Directions*; Wiley-VCH: Weinheim, Germany, 2007.
(6) Chen, X.; Mao, S. S. *Chem. Rev.* **2007**, *107*, 2891.
(7) Cai, Q.; Paulose, M.; Varghese, O. K.; Grimes, C. A. *J. Mater. Res.* **2005**, *20*, 230.
(8) Allam, N. K.; Grimes, C. A. *Sol. Energy Mater. Sol. Cells* **2008**, *92*, 1468.
(9) Allam, N. K.; Grimes, C. A. *J. Phys. Chem. C* **2007**, *111*, 13028.
(10) Rani, S.; Roy, S. C.; Paulose, M.; Varghese, O. K.; Mor, G. K.; Kim, S.; Yoriya, S.; LaTempa, T. J.; Grimes, C. A. *Phys. Chem. Chem. Phys.* **2010**, *12*, 2780.
(11) Varghese, O. K.; Paulose, M.; Grimes, C. A. *Nat. Nanotechnol.* **2009**, *4*, 592.
(12) Ghicov, A.; Schmuki, P. *Chem. Commun.* **2009**, 2791.
(13) Chanmanee, W.; Watcharenwong, A.; Chenthamarakshan, C. R.; Kajitvichyanukul, P.; de Tacconi, N. R.; Rajeshwar, K. *J. Am. Chem. Soc.* **2008**, *130*, 965.
(14) Mor, G. K.; Oomman, K. V.; Paulose, M.; Shankar, K.; Grimes, C. A. *Sol. Energy Mater. Sol. Cells* **2006**, *90*, 2011.
(15) Raja, K. S.; Misra, M.; Paramguru, K. *Electrochim. Acta* **2005**, *51*, 154.
(16) Allam, N. K.; Feng, X. J.; Grimes, C. A. *Chem. Mater.* **2008**, *20*, 6477.
(17) Paulose, M.; Shankar, K.; Yoriya, S.; Prakasam, H. E.; Varghese, O. K.; Mor, G. K.; Latempa, T. J.; Fitzgerald, A.; Grimes, C. A. *J. Phys. Chem. B* **2006**, *110*, 16179.
(18) Allam, N. K.; Grimes, C. A. *J. Phys. Chem. C* **2009**, *113*, 7996.
(19) Allam, N. K.; Grimes, C. A. *Langmuir* **2009**, *25*, 7234.
(20) Allam, N. K.; Shankar, K.; Grimes, C. A. *Adv. Mater.* **2008**, *20*, 3942.
(21) Linsebigler, A. L.; Lu, G.; Yates, J. T. *Chem. Rev.* **1995**, *95*, 735.
(22) Peshkov, V. V.; Milyutin, V. N. *Metalloved. Term. Obrab. Met.* **1984**, *12*, 43.
(23) Varghese, O. K.; Gong, D. W.; Paulose, M.; Grimes, C. A.; Dickey, E. C. *J. Mater. Res.* **2003**, *18*, 156.
(24) Felner, F. P. *Low Temperature Oxidation*; Wiley-Interscience: New York, 1981.
(25) Zhang, H.; Banfield, J. F. *J. Mater. Res.* **2000**, *15*, 437.
(26) Klug, H. P.; Alexander, L. E. *X-ray Diffraction Procedures for Polycrystalline and Amorphous Materials*; Wiley-Interscience: New York, 1974.
(27) Biggs, D. *Handbook of X-ray and Ultraviolet Photoelectron Spectroscopy*; Hayden and Son Ltd.: London, 1977.
(28) Xu, L.; Tang, C.; Qian, J.; Huang, Z. *Appl. Surf. Sci.* **2010**, *256*, 2668.
(29) Diguna, L. J.; Shen, Q.; Kobayashi, J.; Toyoda, T. *Appl. Phys. Lett.* **2007**, *91*, 023116.
(30) Fujishima, A.; Zhang, X.; Tryk, D. A. *Surf. Sci. Rep.* **2008**, *63*, 515.
(31) Nishikiori, H.; Qian, W.; El-Sayed, M. A.; Tanaka, N.; Fujii, T. *J. Phys. Chem. C* **2007**, *111*, 9008.

JP1037014